First Comparison of Sentinel-1 and TerraSAR-X Data in the Framework of Maritime Targets Detection: South Italy Case

Domenico Velotto, *Member, IEEE*, Carlos Bentes, Björn Tings, and Susanne Lehner

***Abstract*—The Sentinel-1A is the first of two satellites that composes the Sentinel-1 radar mission. Both satellites operate a C-band synthetic aperture radar (SAR) system to give continuity to the European SAR program. SAR is a flexible sensor able to fulfil users/applications requirements in terms of resolution and coverage thanks to different operational modes and polarizations. With the in-orbit availability of very-high-resolution X-band SAR sensors, the Sentinel-1 satellites have been designed to achieve wide coverage at medium to high resolution. The interferometric wide swath (IWS) mode implemented with the terrain observation with progressive scan (TOPS) technique is the standard acquisition mode over European waters and land masses. IWS in dual-polarization (VV/VH) combination offers 250-km swath at 5 m × 20 m (range × azimuth) spatial resolution. These specifications are in line with the needs of the European Maritime and Security Agency (EMSA) for oil spill and ship detection applications included in the CleanSeaNet program. The main goals of this paper are: assessment of medium-to-high-resolution C-band Sentinel-1 data with very-high-resolution X-band TerraSAR-X data for maritime targets detection; synergetic use of multiplatforms satellite SAR data for target features extraction; evaluation of polarimetric target detectors for the available co-polarization and cross-polarization Sentinel-1A IWS VV/VH products. The objectives are achieved by means of real, almost coincident C-band and X-band SAR data acquired by Sentinel-1A and TerraSAR-X satellites over Gulf of Naples and Catania (South Italy). Furthermore, the obtained results are supported by recorded ground truth vessel reports via terrestrial automatic identification system (AIS) stations located in the area.**

***Index Terms*—Multifrequency, multipolarization, synthetic aperture radar (SAR), targets detection.**

I. Introduction

With the launch of Sentinel-1A satellite on April 3, 2014 the European Radar Observatory program became operative in the framework of the Copernicus initiative. Copernicus, previously known as Global Monitoring for Environment and Security (GMES), is a joint initiative of the European Commission (EC) and the European Space Agency (ESA) established with the objective of the implementation of services dealing with environment and security [1]. Thanks to the experience gained by working groups in several European Union (EU) projects, in the Copernicus initiative three priority services have been identified: marine, land, and emergency services.

Sentinel-1 is a long-term constellation mission composed of two C-band radar polar orbiting satellites, i.e., Sentinel-1A and Sentinel-1B (launch of the second is scheduled for 2016), that provides continuous all-weather day/night imagery for the following identified applications [1], [2]:

1) land forests, waters, soil, and agriculture monitoring;
2) natural disasters support via emergency mapping;
3) maritime environment monitoring;
4) sea ice and iceberg observation;
5) high-resolution ice charts production;
6) sea and ice condition forecast;
7) oil spills mapping;
8) sea vessel detection;
9) climate change monitoring.

Each of these particular applications has different needs in terms of coverage, spatial resolution, noise floor, and radar polarization. Nevertheless, synthetic aperture radar (SAR) is a flexible sensor able to fulfil users/applications requirements with a single instrument, thanks to the possibility of implementing different operational modes. Recent SAR missions offer also multipolarization (dual- or full-polarization) acquisition capabilities.

With the availability of commercial very-high-resolution X-band SAR sensors like the German TerraSAR-X/TanDEM-X constellation and the Italian Cosmo-SkyMed 4 satellites constellation, Sentinel-1 satellites have been designed to achieve medium-to-high-resolution imaging capabilities and wide coverage. Despite the aforementioned SAR flexibility, wide coverage and very-high-resolution imagery at the same time are not possible with the actual SAR design technology.

Sentinel-1 is the first satellite built with interferometric wide swath (IWS) mode exploiting the terrain observation with progressive scan (TOPS) technique. IWS is the standard acquisition mode over European waters and land masses for both interferometric applications, e.g., digital elevation model (DEM), and maritime surveillance applications, e.g., pollution and vessel monitoring. IWS in dual-polarization (VV/VH) combination offers 250-km swath at 5 m × 20 m (range × azimuth) spatial resolution in single look. These imagery characteristics are in line with the needs of the satellite SAR-based oil pollution and ship detection European CleanSeaNet service established by the European Maritime and Security Agency (EMSA). As a matter of fact, when a single SAR polarization

Manuscript received January 21, 2015; revised June 03, 2015, September 11, 2015, and December 08, 2015; accepted January 15, 2016. Date of publication April 05, 2016; date of current version October 11, 2016.

Associate Editor: R. Romeiser

The authors are with the Maritime Security Lab, Remote Sensing Technology Institute, German Aerospace Center, Bremen 28199, Germany (e-mail: Domenico.Velotto@dlr.de; Carlos.Bentes@dlr.de; Bjoern.Tings@dlr.de; Susanne.Lehner@dlr.de).

Digital Object Identifier 10.1109/JOE.2016.2520216

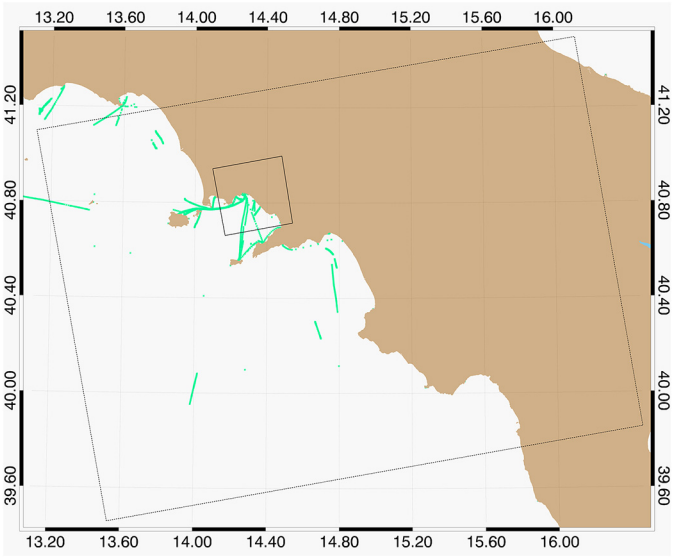

Fig. 1. Collected AIS messages (green dots) inside the boundary box given by the acquired Sentinel-1 (dashed black line) and TerraSAR-X (continuous black line) SAR data over Gulf of Naples, Italy. The time span is approximately 1 h before and 0.5 h after the satellite overpasses.

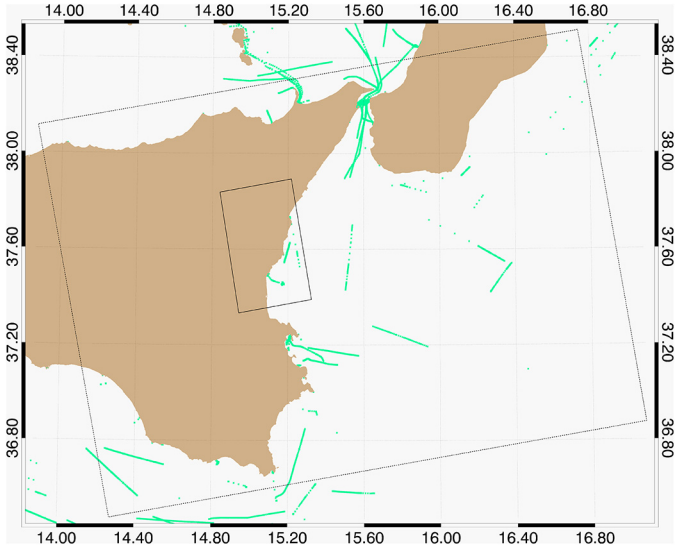

Fig. 2. Collected AIS messages (green dots) inside the boundary box given by the acquired Sentinel-1 (dashed black line) and TerraSAR-X (continuous black line) SAR data over Catania, Italy. The time span is approximately 1 h before and 0.5 h after the satellite overpasses.

is available, VV polarization is the preferred choice for oil spill detection algorithms and HH polarization is preferred for ship detection algorithms [3]. In [4], the potential use of SAR cross-polarization combination (HV or VH) for ship detection is discussed and shown to be useful especially at low incidence angles. On the other hand, while spatial resolution is less important than coverage for SAR oil spill detection, it is a critical parameter for both ship detection (regarding small vessels as fishing boats) and classification. In conclusion, taking into account complementary very-high-resolution X-band satellite SAR data as support for specific application needs, the choice of medium-to-high resolution C-band dual-polarization VV/VH as default product mode over European's water seems a good tradeoff among SAR maritime services prerequisites.

Due to the fact that Sentinel-1A and TerraSAR-X have different orbit characteristics (the first has a mean height of 693 km with a repeat cycle of 12 days; the second has a mean height of 515 km with a repeat cycle of 11 days), an area on Earth can be monitored from space at different times, with different geometries, resolution, and coverage. Despite Sentinel-1A fixed acquisition plan over European waters, TerraSAR-X acquires data on-demand and has a fast satellite commanding (e.g., emergencies cases). Thanks to these properties and the aforementioned complement between the two satellites, Sentinel-1A and TerraSAR-X form an interesting tandem for maritime surveillance applications. Therefore, within this paper, the following objectives have been identified:

1) assessment of the operational IWS C-band Sentinel-1 with StripMap X-band TerraSAR-X data for maritime targets detection;
2) synergetic use of multiplatforms satellite SAR data for targets cross checking and vessel speed estimation;
3) first evaluation of polarimetric target detectors for the available co-polarization and cross-polarization Sentinel-1A IWS products, previously demonstrated for RADARSAT-2 high-resolution quad-pol and very-high-resolution dual-pol TerraSAR-X data [5], [6].

The aims are achieved by means of real, almost coincidental C-band and X-band SAR data acquired by Sentinel-1A and TerraSAR-X satellites. On November 25, 2014, just a few months after Sentinel-1A concluded the commissioning phase, there was an opportunity to command TerraSAR-X acquisitions in the southern part of Italy, very close in time to the planned Sentinel-1A [1], [2]. During these controlled experiments, ground truth data provided by terrestrial automatic identification system (AIS) vessel reports have been recorded approximately 1 h before and 0.5 h after SAR acquisitions. AIS data are used to validate the objectives posed for this paper.

The paper is organized as follows. Section II contains details on the material and data analyzed. Section III is dedicated to the listed purposes 1 and 2. Section IV is dedicated to the listed purpose 3 where the theory and results on polarimetric detectors are presented; discussion and conclusions are sketched in Section V.

II. Material and Data Description

In this section, the material and the data analyzed for the purposes of this paper are introduced and described. Used material consists of satellite SAR data acquired in C- and X-band by two different satellites, and terrestrial AIS reports broadcast by ships in the area given by the satellites footprint on ground. The AIS data set is used to identify most of the maritime targets imaged by SAR and hence represents, for those targets, the ground truth. Therefore, it is worth a short introduction to the terrestrial AIS system before proceeding with SAR data description.

AIS is a messaging system developed for collision avoidance and to support other navigation systems, e.g., marine

TABLE I
SAR DATA DESCRIPTION

Dataset *Name*	**Data ID** *Time*	**Resolution (m)** *Rg × Az*	**Inc. Angle (°)** *Nr - Fr*	**Ground Range Coverage** *km*	**Frequency** *Band*	**Polarization** *T/R*	**Wind** m/s
Gulf of Naples	2014/11/25 *16:50* Z	1.2 × 3.3	27.2 – 30.3	32.1	**X**	**HH**	< 2
	2014/11/25 *16:57* Z	2.7-3.5 × 21.7	30.0 – 46.0	251.8	**C**	**VV/VH**	
Gulf of Catania	2014/11/25 *16:49* Z	1.2 × 3.3	26.9 – 30.3	34.3	**X**	**HH**	3-6
	2014/11/25 *16:56* Z	2.7-3.5 × 21.7	30.0 – 46.0	251.8	**C**	**VV/VH**	

radars, long range identification and tracking (LRIT) systems and vessel traffic service (VTS). Vessels obliged to transmit the message via AIS system are: ships of any type exceeding 300 tons engaged in international voyages, cargo ships exceeding 500 tons, and passenger vessels [7]. Lately, to contrast the large numbers of collisions involving fishing vessels, the EU has amended the Directive 2002/59/EC on the vessel traffic monitoring and information system, proposing that fishing vessels greater than 15 m sailing in European waters be fitted with AIS [8]. Other maritime targets that might be equipped with AIS and broadcast their message are: wind turbines, navigation aids, buoys, etc. Broadcast rate is variable (from seconds to minutes) and depends on the maritime target status, e.g., at anchor, sailing, maneuvering, etc., and AIS message type. Information sent jointly with geographical location are: International Maritime Organization (IMO) number, call sign, maritime mobile service identity (MMSI), speed and course over ground (CoG). Additional vessels' features are: ship name size, type, estimated time of arrival (ETA), and destination. The latter are usually set manually and therefore often unreliable and/or not available. AIS transponder broadcasts in VHF frequency achieving horizontal range of circa 70 km. Satellite reception of AIS signals is possible but here only terrestrial AIS information is exploited. It is evident that not all SAR detected maritime targets could be matched with a valid AIS message. Moreover, due to the fact that SAR is a radar imaging system that takes a snapshot of the observed scene in few seconds, there might be still a time mismatch. For these reasons, the strategy used is to visually confirm automatic colocated AIS data with SAR detections using additional historical AIS data in the time range span of approximately 1 h before and 0.5 h after satellite overpasses. Figs. 1 and 2 show the AIS messages (green dots) collected over the two areas where Sentinel-1A (dashed black line) and TerraSAR-X (continuous black line) data have been acquired. Some shipping route, e.g., between main land and the islands in the Gulf of Naples or in the Strait of Sicily, is clearly visible. Due to the different ground coverage between the Sentinel-1A's IWS mode and the TerraSAR-X's StripMap mode, the multifrequency assessment could be done only in the overlapping area and where targets could be identified with AIS data (see Figs. 1 and 2).

To preserve the original sensors' resolution, both C- and X-band SAR data sets are processed starting from single look complex (SLC) format and slant range geometry. Table I provides a summary of data characteristics corresponding to each acquired data set. It is worth noticing that TerraSAR-X imagery has been planned in HH polarization since it was known that Sentinel-1A would provide the combination VV/VH. Fig. 3 (Fig. 4) shows color-coded ground projection of the SAR data set named in Table I Gulf of Naples (Gulf of Catania). The left panel is the Sentinel-1 IWS VV/VH polarization (RGB color coding is with $\mathrm{R} = \langle|\boldsymbol{VV}|\rangle$, $\mathrm{G} = \langle|\boldsymbol{VH}|\rangle$, and $\mathrm{B} = \langle|\boldsymbol{VV} - \boldsymbol{VH}|\rangle$) acquired on November 25, 2014 at 16:57 Z (November 25, 2014 at 16:56 Z). The right panel is TerraSAR-X HH polarization (RGB color coding is given by $\mathrm{R} = \boldsymbol{std}(|\boldsymbol{HH}|)$, $\mathrm{G} = \boldsymbol{w}_1\langle|\boldsymbol{HH}|\rangle$, and $\mathrm{B} = \boldsymbol{w}_2\langle|\boldsymbol{HH}|\rangle$) acquired on November 25, 2014 at 16:50 Z (November 25, 2014 at 16:49 Z). The weights $\boldsymbol{w}_1$ and $\boldsymbol{w}_2$ are chosen to take into account low and high range variation of the radar amplitude, while $std(\cdot)$, $\langle\cdot\rangle$, and $|\cdot|$ are the standard deviation, average, and absolute value operators, respectively. Acquisitions time differences are about 7 min; both satellite orbits are ascending.

III. C-/X-BAND ANALYSIS AND SYNERGY

Sentinel-1A IWS SLC products are distributed as individually focused complex burst images into three single subswath images (three images for single polarization and six images for dual polarization). Each subswath, namely IW1, IW2, and IW3, has been processed individually (reading, de-bursting, and calibration) and merged at the last stage to produce the map in the left panels of Figs. 3 and 4. The strategy to process subswaths individually is kept also when running target detection algorithms (and additional polarimteric features extraction). This enables the parallelization of algorithms and the achievement of near-real-time (NRT) services, otherwise difficult due to the large amount of data given by IWS SLC products.

Three interesting cases have been chosen for the C-/X-band assessment and synergy with regard to maritime targets detection and surveillance: 1) monitoring of harbor area; 2) analysis of ships and ship wake signatures; and 3) surveillance of small boats without AIS.

A. Monitoring of Harbor Area

Monitoring of harbors from space can be quite a challenging task. Very-high-resolution imageries are usually preferred for

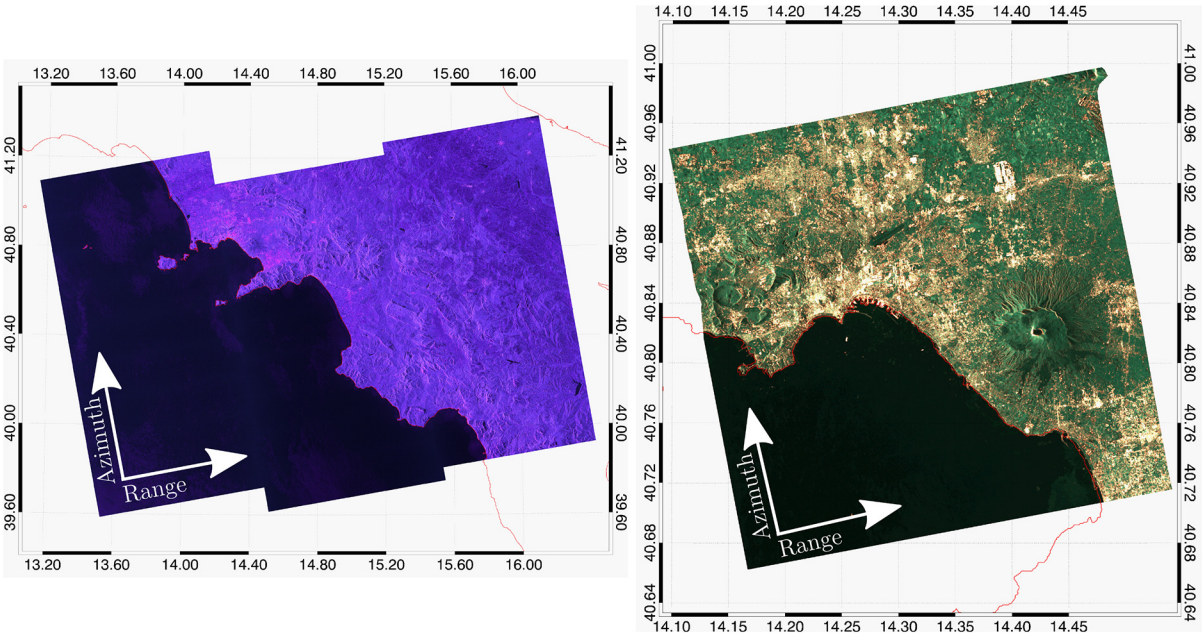

Fig. 3. RGB color-coded representation of the SAR data acquired by Sentinel-1 in IWS dual-polarization VV/VH with $\mathrm{R} = \langle |VV| \rangle$, $\mathrm{G} = \langle |VH| \rangle$, and $\mathrm{B} = \langle |VV - VH| \rangle$ (left) and TerraSAR-X StripMAP single-polarization HH with $\mathrm{R} = std(|HH|)$, $\mathrm{G} = w_1 \langle |HH| \rangle$, and $\mathrm{B} = w_2 \langle |HH| \rangle$ (right) over the Gulf of Naples, Italy.

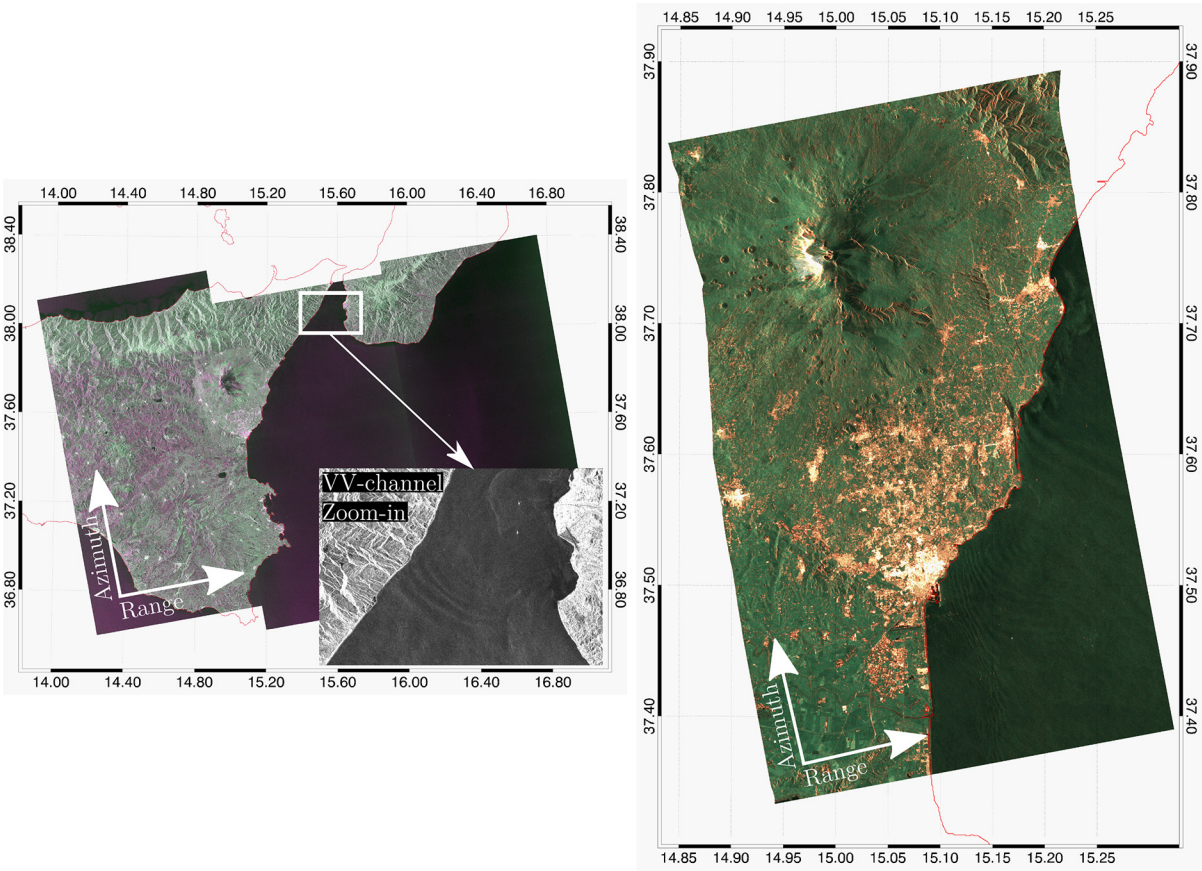

Fig. 4. RGB color-coded representation of the SAR data acquired by Sentinel-1 in IWS dual-polarization VV/VH with $\mathrm{R} = \langle |VV| \rangle$, $\mathrm{G} = \langle |VH| \rangle$, and $\mathrm{B} = \langle |VV - VH| \langle$ (left) and TerraSAR-X StripMAP single-polarization HH with $\mathrm{R} = std(|HH|)$, $\mathrm{G} = w_1 \langle |HH| \rangle$, and $\mathrm{B} = w_2 \langle |HH| \rangle$ (right) over Catania, Italy.

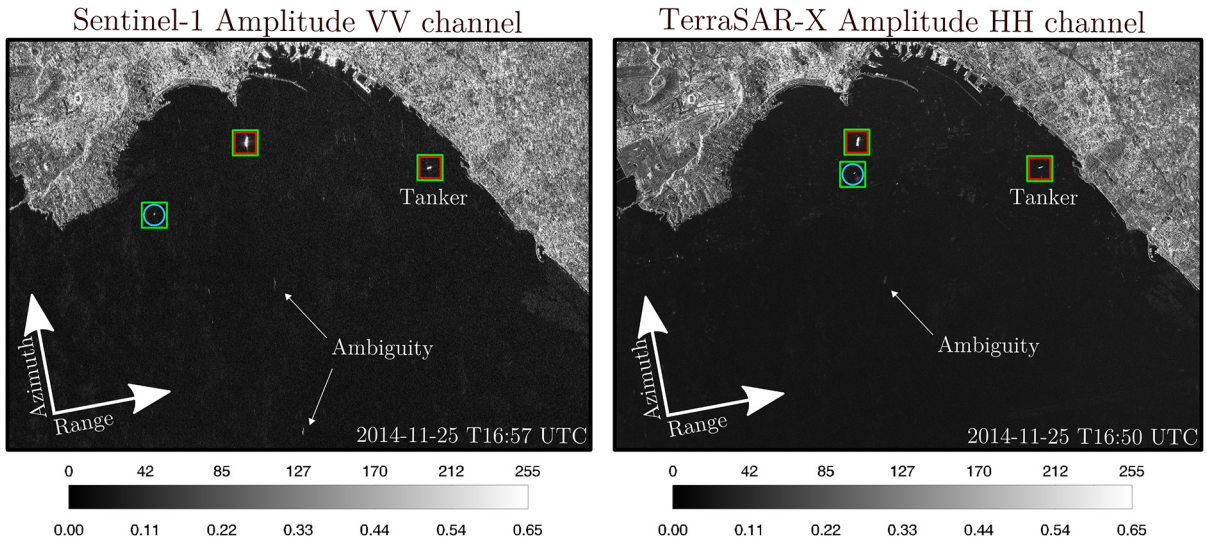

Fig. 5. Closeup of Fig. 3, showing Naples's harbor: Sentinel-1 acquired on November 25, 2014 at 16:57 Z, VV polarization calibrated amplitude (left); TerraSAR-X acquired on November 25, 2014 at 16:50 Z, HH polarization calibrated amplitude (right). Red rectangles are nonmoving marine targets; blue circles are moving marine targets; green rectangles are targets identified by valid AIS message.

this kind of application. Nevertheless, the very-high-resolution SAR data have a limited coverage and the contextual surrounding information is unknown by this means.

Referring to the TerraSAR-X in Fig. 3 (right panel), one can notice a very smooth ocean radar signature in the Gulf of Naples. Having a look at Sentinel-1A imagery acquired after few minutes (Fig. 3, left panel) it is possible to gather that a low meteo-ocean condition is in place all over the bay. This information has been confirmed by auxiliary satellite wind speed measurements and wind speed model data with an average speed below 2 m/s. Similarly, it can be deduced that the internal wave signatures on TerraSAR-X (Fig. 4, right panel) near Catania's harbor are probably originated in the Strait of Messina (where internal wave signatures are also present on Sentinel-1A image in Fig. 4, left panel) and propagating north–south along the coast [9]. In the context of harbor monitoring by means of very-high-resolution satellite SAR imagery, e.g., TerraSAR-X, the possibility to gather large-scale meteo-ocean information by means of complementary wide swath satellite SAR imagery, e.g., Sentinel-1A, is highly desired. In this sense, Sentinel-1 mission will boost such developments thanks to ESA Sentinel-1 mission's free data policy.

In Fig. 5, Naples's harbor, imaged by Sentinel-1 (left panel) and TerraSAR-X (right panel), is shown.

Both subscenes are ground projected and North oriented (satellite orientation is indicated by the arrows range and azimuth). The calibrated amplitude of the respective co-polarization channels (VV for Sentinel-1A and HH for TerraSAR-X) is displayed in Fig. 5. The same histogram scaling is applied in order to have equal visual information content. Speckle is mitigated using a boxcar filter with kernel dimensions adapted to the different resolutions in range and azimuth direction (5×3 in range $\times$ azimuth). These processing steps are used for all cases shown in this section, unless explicitly stated.

Three marine targets are identified as ships by colocated AIS messages (green rectangles); two of them are nonmoving (red rectangles) and one is moving (blue circle). Due to the low ocean clutter both subscenes are affected by azimuth ambiguities. Ships or harbor structures ghosting on the ocean surface is a major problem when dealing with SAR ship detection. These artefacts are often causing false alarms. To mitigate this problem, several methods have been proposed and used in literature for single- and multiple-polarization SAR data [10]–[15]. With both data sets being not fully polarimetric, azimuth ambiguities are removed after ship detection in a postprocessing step which exploits the fixed azimuth and range distance of the ghosts from real targets [10].

The multifrequency analysis of the ship radar signature is conducted taking as example the tanker ship at anchor in the Gulf of Naples in Fig. 5. It is an oil/chemical tanker of dimensions: 144-m length and 23-m breadth. This target has been selected because it is almost perfectly aligned in its length axis with the radar range direction. Furthermore, being the target at anchor, it is assumed that the influence caused by different viewing geometry between the C-/X-band acquisitions is negligible (although with a small difference in incidence angle; see Table I). A pictorial profile of a typical oil/chemical tanker is illustrated in Fig. 6(a), where the main structures are indicated with letters from A to E. Fig. 6(b)–(c) shows the color-coded C-band radar signature acquired by Sentinel-1A in the VV and VH polarizations, respectively. On the other hand, Fig. 6(d) shows the color-coded X-band radar signature acquired by TerraSAR-X in the HH polarization. A common byte scaling is applied to the amplitude measurements across the data set to facilitate the analysis. It is easy to recognize in Fig. 6(b) five strong backscattering points along the tanker length axis, which distribution fits reasonably well with the main structures A–E indicated in Fig. 6(a). These signatures are due to a mixture of direct reflections from the metallic constructions, e.g., crane, bridge, etc., and double-bounce between them and the deck. This is further confirmed by the VH polarization signature in Fig. 6(c) which is more an indication of volume scattering rather than direct or double bounce. The X-band co-polarization

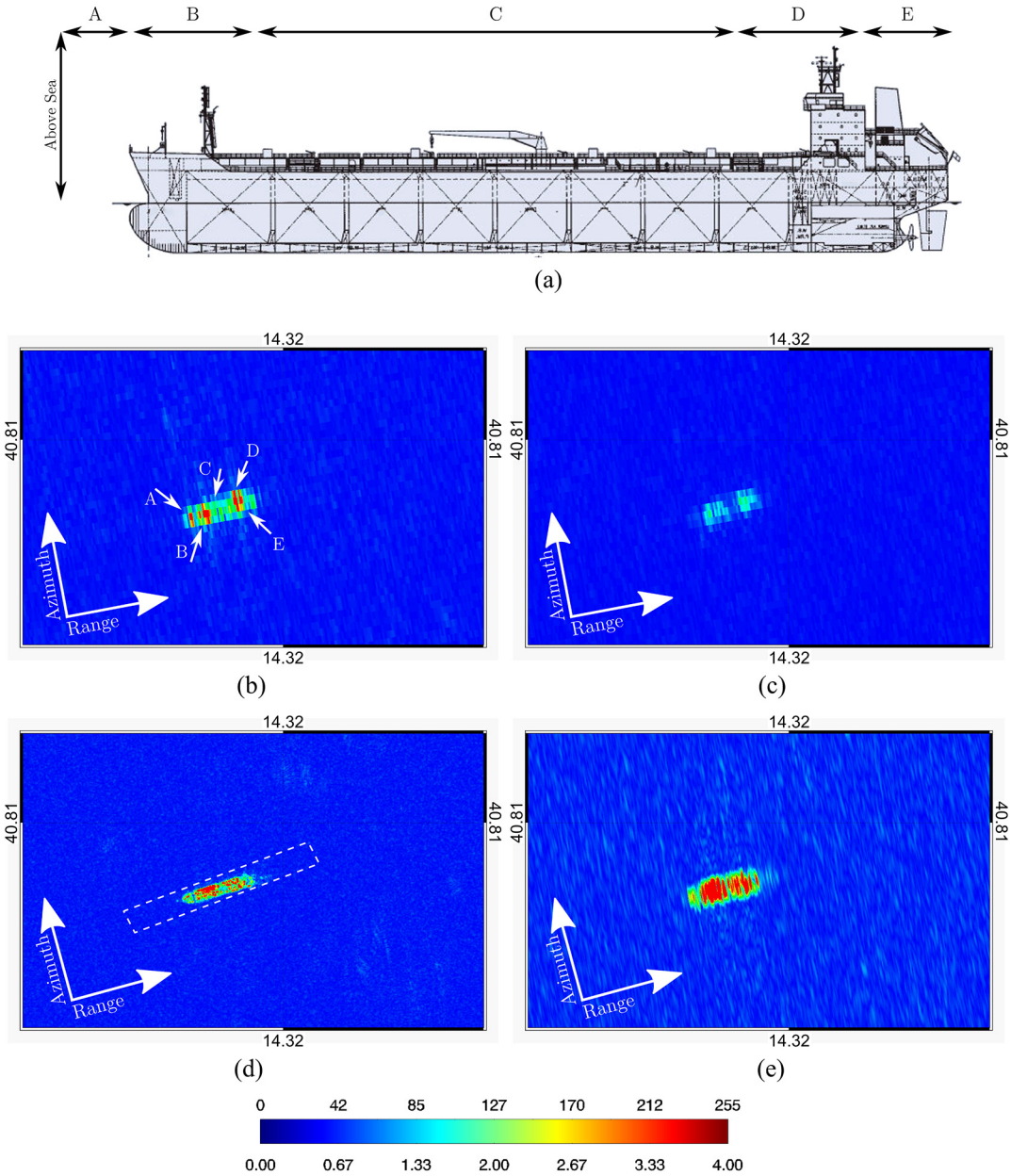

Fig. 6. Multifrequency radar signature of a tanker ship at anchor in Gulf of Naples (see Fig. 5). All SAR images are ground projected with pixel spacing according to the sensor's resolution (see Table I). (a) Typical tanker's profile of the type analyzed here. (b) Sentinel-1A C-band VV-polarization. (c) Sentinel-1A VH-polarization. (d) TerraSAR-X X-band HH-polarization. (e) TerraSAR-X X-band HH-polarization with azimuth resolution reduced to match the one of the Sentinel-1A.

(HH) radar signature in Fig. 6(d) is different from the C-band co-polarization (VV) in Fig. 6(b). Unlike what has been highlighted for C-band VV polarization, a diffuse distribution of strong backscattering points along the tanker length axis is in place at X-band [Fig. 6(d)].

The factors that might produce such behavior in the target signatures at C- and X-bands are: 1) different radar illumination geometry; 2) different polarization; 3) different resolution; and 4) different frequency. The first factor is excluded *a priori* since the target is at anchor (according to the AIS message received) in the harbor area and imaged by the two satellites with similar orbit heading in a short time difference (hence possible target's pitch, roll, and yaw are assumed negligible). Regarding the polarization's influence, having the target at width of 23 m, it is reasonable to assume that the dihedrals responsible for the double bounce (usually the stronger contribution) have a comparable vertical and horizontal size making the radar response quasi polarization independent. In [16], the influence of the factors 1) and 2) have been further analyzed for different types of ships (tanker and cargo), where the Sentinel-1A and TerraSAR-X data have the same polarization and illumination geometry. The conclusions in [16] confirm the assumptions made here. Concerning the resolution influence, being the marine target oriented with the major and minor axes in SAR range–azimuth directions [see Fig. 6(b)–(d)], it can be discussed individually along these directions. The strong azimuth resolution difference between the C- and X-band SAR data ($\sim$ 21 m and

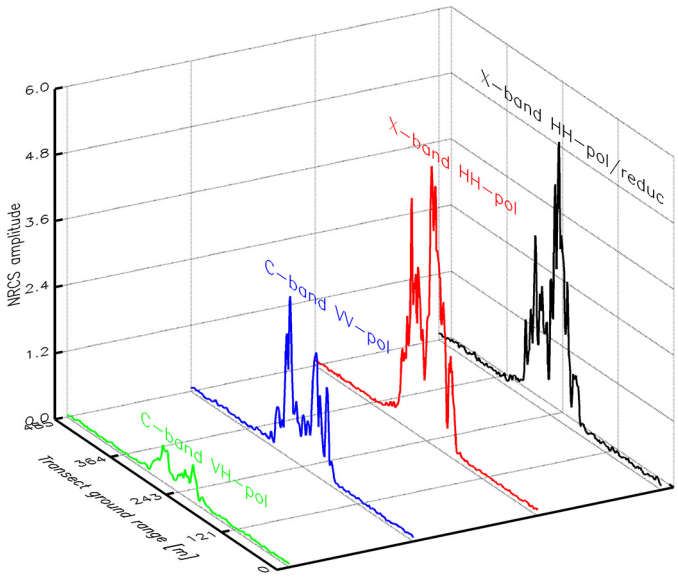

Fig. 7. Tanker ship profiles along the radar viewing direction for different frequency and polarization.

$\sim$ 3 m, respectively) is evident comparing Fig. 6(b) and (d). The tanker's width signature appears in C-band just in few pixels in azimuth direction while in X-band much more details are provided. On the other hand, the comparable resolution in range of the C- and X-band SAR data ($\sim$ 2 m and $\sim$ 1 m, respectively) does not fully justify the different texture in the radar signature along range direction (along the major axis of the tanker). To further investigate this point, an X-band data set with reduced azimuth resolution (down to $\sim$ 21 m as for the C-band data set) has been generated from the original X-band TerraSAR-X product by extracting a sublook with reduced azimuth processed bandwidth, i.e., 1-look with smaller illumination time, via time-frequency analysis. The output of this process is shown in Fig. 6(e), which can be directly compared with Fig. 6(b). Even though range and azimuth resolutions are in this case similar, the different radar signature in range persists. To easily compare the radar range signatures at different frequency and resolution, the data extracted from the region given by the dashed white frame in Fig. 6(d) are plotted (after being averaged in azimuth direction) in Fig. 7 for the case of Fig. 6(b)–(e). Comparing the target range profiles in Fig. 7 it can be observed that resolution does not play a major role. Considering, for example, the main deck of the target under analysis (which corresponds to the area around the 243 m of the transect ground range size in Fig. 7), the radar response in C-band (blue curve in Fig. 7) is quite low with no significant texture, i.e., mostly specular reflection, while both original and reduced resolution X-band data sets (red and black curve in Fig. 7) show noticeable texture in the radar response. As an outcome of this analysis, it is possible to conclude that among the four factors listed, the different working frequencies play the major role in the diverse radar backscatter signatures of the tanker ship observed in Sentinel-1A and TerraSAR-X. Hence, the different information provided by the Sentinel-1A and TerraSAR-X satellite can be exploited to help marine target classification. An applicative example is provided in [16] where a ship located in the coastal zone close to a harbor (non-reporting its status via AIS) could be analyzed at C- and X-band frequency and we conclude that it is probably a cargo at anchor.

It must be noted that previous works in the literature have shown the potential improvements for ship detection application when combining satellite meter-resolution X-band SAR data with optical images [17] or airborne centimeter-resolution X-band data [18]. Monitoring of harbor area making use of multiple SAR satellite operating at different frequencies is therefore here first investigated. The findings in the C-/X-band analysis of the tanker ship are in partial agreement with the multifrequency vessel scattering simulations provided in [19] for two fishing vessels and a passenger ferry. From these simulations, a stable radar backscatter along the frequency span (including C- and X-band) has been observed. Such stability has not been encountered in this study when analyzing the backscatter of a tanker in real C- and X-band SAR data. This is probably due to the fact that oil/chemical tankers usually carry complex metallic structures on their deck, formed by pipelines and cranes, which are normally not present in fishing and ferry vessels. Furthermore, it was observed that the backscatter of a tanker ship in the original and reduced resolution X-band data does not change the fundamental properties characterizing the scattering map of the ship. This observation is in agreement with the outcomes of the downscaling procedure applied at high frequency to the ship's model (which is equivalent to reducing the sensor's resolution) for the simulations of the vessel scattering maps in [19].

B. *Analysis of Ships and Ship's Wake Signatures*

This case has been chosen because ship wake detection is often desired when dealing with SAR marine target detection. In fact, ship wakes might be used to identify moving from non-moving marine targets and to help in detecting small boats for cases where only the wake signature is visible on the ocean surface. In Fig. 8, moving maritime targets (blue circles) identified with AIS (green rectangles) as imaged by Sentinel-1 (left panel) and TerraSAR-X (right panel) are shown. Reported AIS ship types for the two targets in Fig. 8 are: the service vessel (length 61 m) and the fishing vessel (length not reported).

Ship's wake signature on radar imagery is still an open and not fully understood process. The influence of the wind-wave field on the ship wake signature in TerraSAR-X imagery has been carried out in [20] with a pilot experiment that makes use of joint radar and sonar measurements of the wake signature. A multifrequency airborne observation of ship wake has been conducted in [21] using P-, L-, and C-band SAR data taken by NASA/JPL DC-8 Airsar. In [22], it was reported that wakes associated with fishing vessels show different wake opening angles in the P- and L-band images and no wake in the C-band image for wind speed regime < 2 m/s. In the case of Fig. 8, it can be noted that for both Sentinel-1A (left) and TerraSAR-X (right) no wake is clearly visible for the service vessel. This might be due to the low ship speed (AIS reported speed is 3.6 kn) as wind speed is between 3 and 6 m/s. On the other hand, the wake of the fishing vessel shows different signatures between Sentinel-1A (left) and TerraSAR-X (right) imagery as shown in

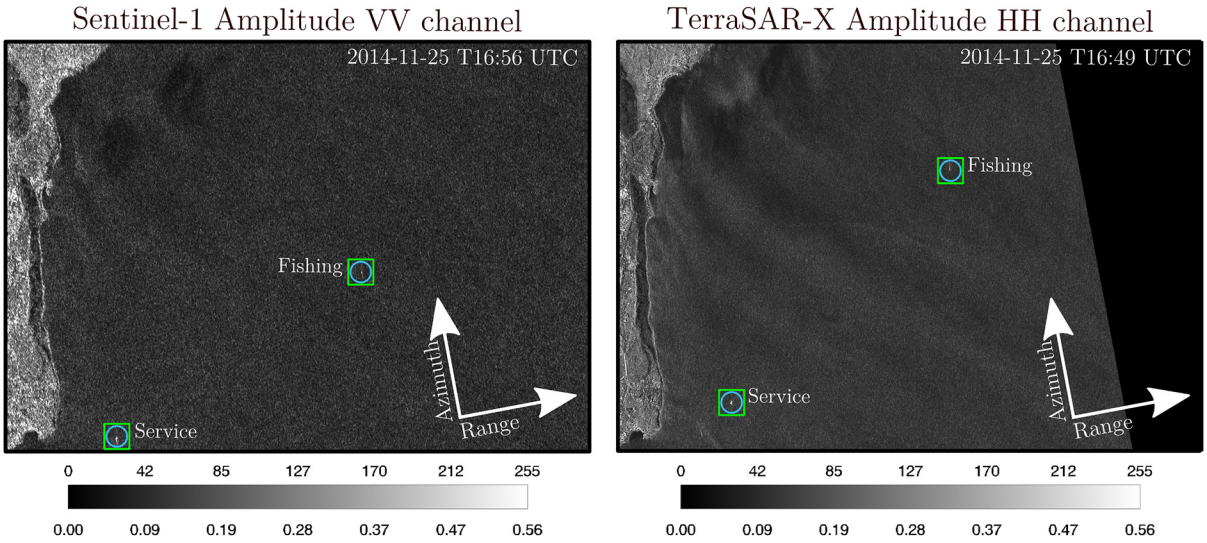

Fig. 8. Closeup of Fig. 4 showing an area North of Catania city with ships and ship's wake signatures: Sentinel-1 acquired on November 25, 2014 at 16:56 Z, calibrated amplitude VV channel representation (left); TerraSAR-X acquired on November 25, 2014 at 16:49 Z, calibrated amplitude HH channel representation (right). Blue circles are moving marine targets; green rectangles are targets identified by valid AIS message.

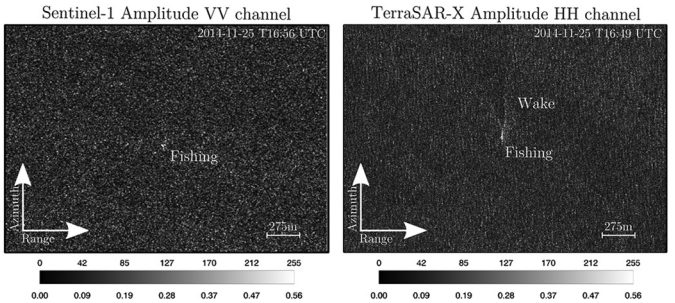

Fig. 9. Full resolution clips showing details of the fishing vessel in Fig. 8 in satellite range–azimuth coordinates; C-band Sentinel-1 (left), X-band TerraSAR-X (right).

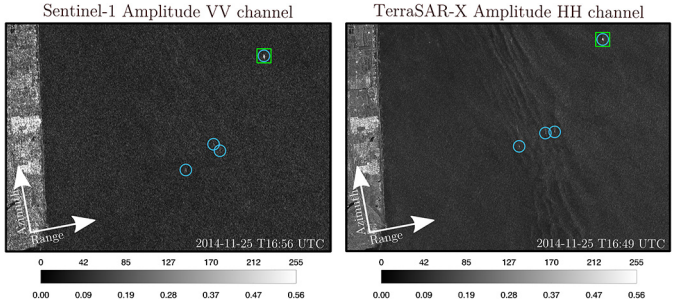

Fig. 10. Closeup of Fig. 4 showing an area south of Catania city with small boats: Sentinel-1 acquired on November 25, 2014 at 16:56 Z, calibrated amplitude VV channel representation (left); TerraSAR-X acquired on November 25, 2014 at 16:49 Z, calibrated amplitude HH channel representation (right). Blue circles are moving marine targets; green rectangles are targets identified by valid AIS message.

details in Fig. 9. The fishing vessel is in the middle of the subscenes and the area around has approximately the same size. The reported AIS speed of the fishing vessel is 9.1 kn and is kept almost constant during the two satellite overpasses. Although the X-band SAR data have been acquired in HH polarization, the fishing vessel wake signature is more pronounced than in C-band (acquired in VV, which is the preferred polarization for SAR wake detection). The lower incidence angle in the X-band band data might play a role in this case.

SAR ship wake detection is usually combined with SAR ship detection to estimate the radial velocity component of moving targets exploiting the Doppler shift effect [22], [23]. This approach cannot be used in the case of SAR imagery with no clear ship wake signature and/or ship moving in direction parallel to the sensor, i.e., azimuth. Such a case is actually given in Fig. 9. Nevertheless, exploiting the availability of multiple images at different acquisition times, classification between moving and nonmoving targets, as well as the estimation of their speed can still be done under certain assumptions. As an example of joint use of Sentinel-1 and TerraSAR-X, the fishing vessel speed has been measured applying a basic change detection algorithm, assuming a linear trajectory at constant speed. The azimuth time difference between the two target positions is about 420 s, while the distance traveled is about 2024 m. This gives an average speed of 9.37 kn that compares well with 9.1 kn reported by the AIS message.

C. Surveillance of Small Boat Without AIS

Because SAR is a synoptic noncooperative surveillance tool, it is mostly useful in the framework of maritime target detection to monitor ships that voluntarily (involved in illegal activity, AIS broadcast not mandatory, fishermen hiding their fishing zone to other fishing vessels, etc.) or involuntarily (not engaged in voyages, AIS, and/or other anticollision system malfunctions, etc.) do not report their positions. Small boats and pleasure crafts often do not use anticollision systems, like AIS, making their position unknown to other ships, especially at nighttime or in foggy conditions.

This is the case of Fig. 10 where three small boats (blue circles) are visually detected in high-resolution C-band VV polarization Sentinel-1A image (left) and very-high-resolution X-band HH polarization TerraSAR-X image (right). It must be pointed out that the visual detection of the three small boats in Sentinel-1A image has been possible thanks to the support of the very-high-resolution TerraSAR-X image acquired

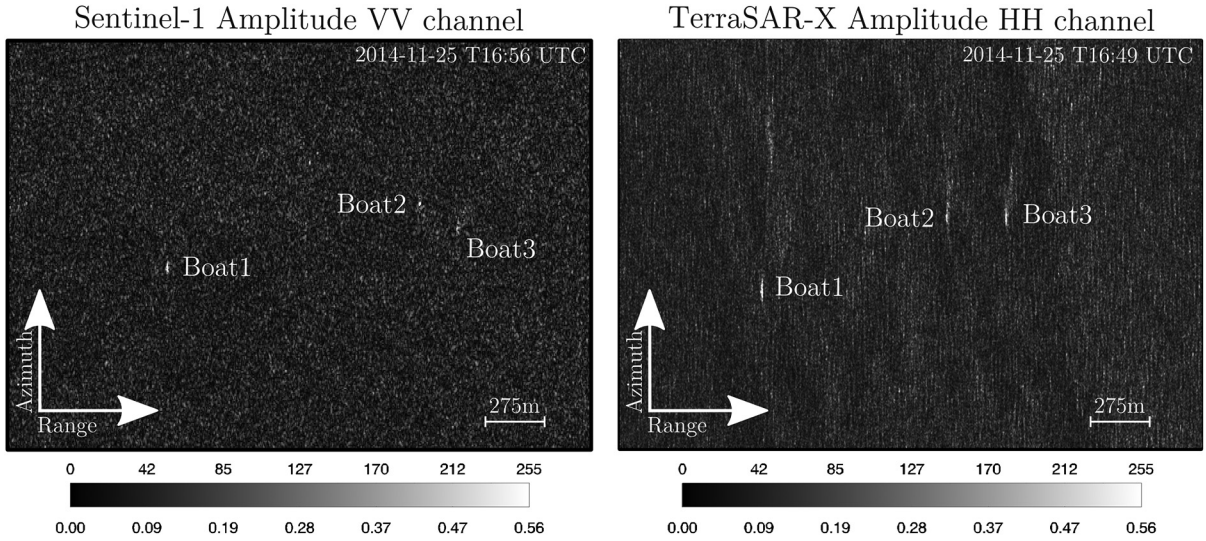

Fig. 11. Full resolution clips showing details of the small boats without AIS in Fig. 10 in satellite range–azimuth coordinates; Sentinel-1 (left), TerraSAR-X (right).

shortly before. This is evident looking at Fig. 11 where full resolution clips of the C-band and X-band data set are shown in the azimuth–range coordinate without interpolation of ground projection processing.

Unfortunately, the size and type of these maritime targets are unknown. To infer the minimum ship size detectable, some work has been done taking into account met-ocean conditions and SAR system design, using C-band data [24] and more recently X-band data [25]. Besides the detection of maritime targets it is often desired to estimate their parameters, e.g., length, width, heading, etc., based on their radar imagery signature. The motion of the small boats in Fig. 11 (as well as for the fishing vessel in Fig. 9) along the satellite azimuth direction produces a SAR imaging artefact, known as the smearing effect, resulting in an elongated shape of the targets. This effect introduces an error when estimating ship parameters [26]. In [26], a methodology has been proposed to reduce this estimation error for different types of SAR products (from medium to very high resolution) using a valuable data set of TerraSAR-X imagery and colocated AIS messages. Applying the same method and assumptions described in the previous section, the speeds of the three targets named Boat1, Boat2, and Boat3 in Fig. 11 have been retrieved. Azimuth time difference for the three targets is about 414 s (they are approximately at the same azimuth line and there are a few milliseconds difference between the three) while the distances traveled are about 750, 377, and 616 m, respectively. These give an average measured speed of about 3.5 kn for Boat1, 1.8 kn for Boat2, and 2.9 kn for Boat3.

IV. Polarimetric Detector: Theory and Results

A first analysis of ship detectability on Sentinel-1 IWS dual-polarimetric products has been carried out in [27] as an extension of the modeling developed in [24] for RADARSAT-1, RADARSAT-2, and Envisat ASAR image data. The model proposed in [27] predicts the minimum ship length considering each polarization available. When comparing model results for co-polarization and cross-polarization IWS products, one of the findings is that ship detection performance at cross-polarization is comparable to the ones at co-polarization [27]. This result is probably due to the IWS incidence angle range as cross-polarization benefits for ship detection are more important at smaller incidence angles [5], [27]. Nevertheless, the promising results obtained by using the polarimetric reflection symmetry properties of maritime targets and ocean clutter for C-band [5] and X-band [6] data suggest evaluating this approach for Sentinel-1A IWS products. In addition, the polarimetric entropy H is extracted from dual-polarimetric covariance matrix and used as a comparison parameter. A ship detector based on the entropy H retrieved from full-polarimetric airborne SAR data was first proposed in [28].

A. Reflection Symmetry Approach

The dual-polarimetric measurements available on Sentinel-1A IWS products can be expressed in terms of the scattering vectors $k_{DH} = (S_{HH}, S_{HV})^T$ or $k_{DV} = (S_{VH}, S_{VV})^T$ depending on the acquired polarization combination. In this paper, Sentinel-1A IWS VV/VH data are analyzed, therefore the 2×2 covariance matrix is defined as

$$\mathrm{C}_2 = \langle k_{DV} \cdot {k_{DV}}^{*T} \rangle = \begin{pmatrix} \langle |S_{VH}|^2 \rangle & \langle S_{VH} S_{VV}^* \rangle \\ \langle S_{VV} S_{VH}^* \rangle & \langle |S_{VV}|^2 \rangle \end{pmatrix}. \quad (1)$$

The reflection symmetry property implies that the unnormalized correlation between co-polarization and cross-polarization channels vanishes for symmetric targets (such as the sea surface) and is different from zero for nonsymmetric targets (such as maritime targets) [5], [6]

$$\begin{cases} \langle S_{VV} S_{VH}^* \rangle = \langle S_{VH} S_{VV}^* \rangle \approx 0, & \text{if target is symmetric} \\ \langle S_{VV} S_{VH}^* \rangle = \langle S_{VH} S_{VV}^* \rangle \neq 0, & \text{if target is not symmetric} \end{cases} \quad (2)$$

Hence, for the following analysis, the modulus of the unnormalized correlation between co-polarization and cross-polarization channels is used as detector:

$$r = |\langle S_{VV} S_{VH}^* \rangle| . \quad (3)$$

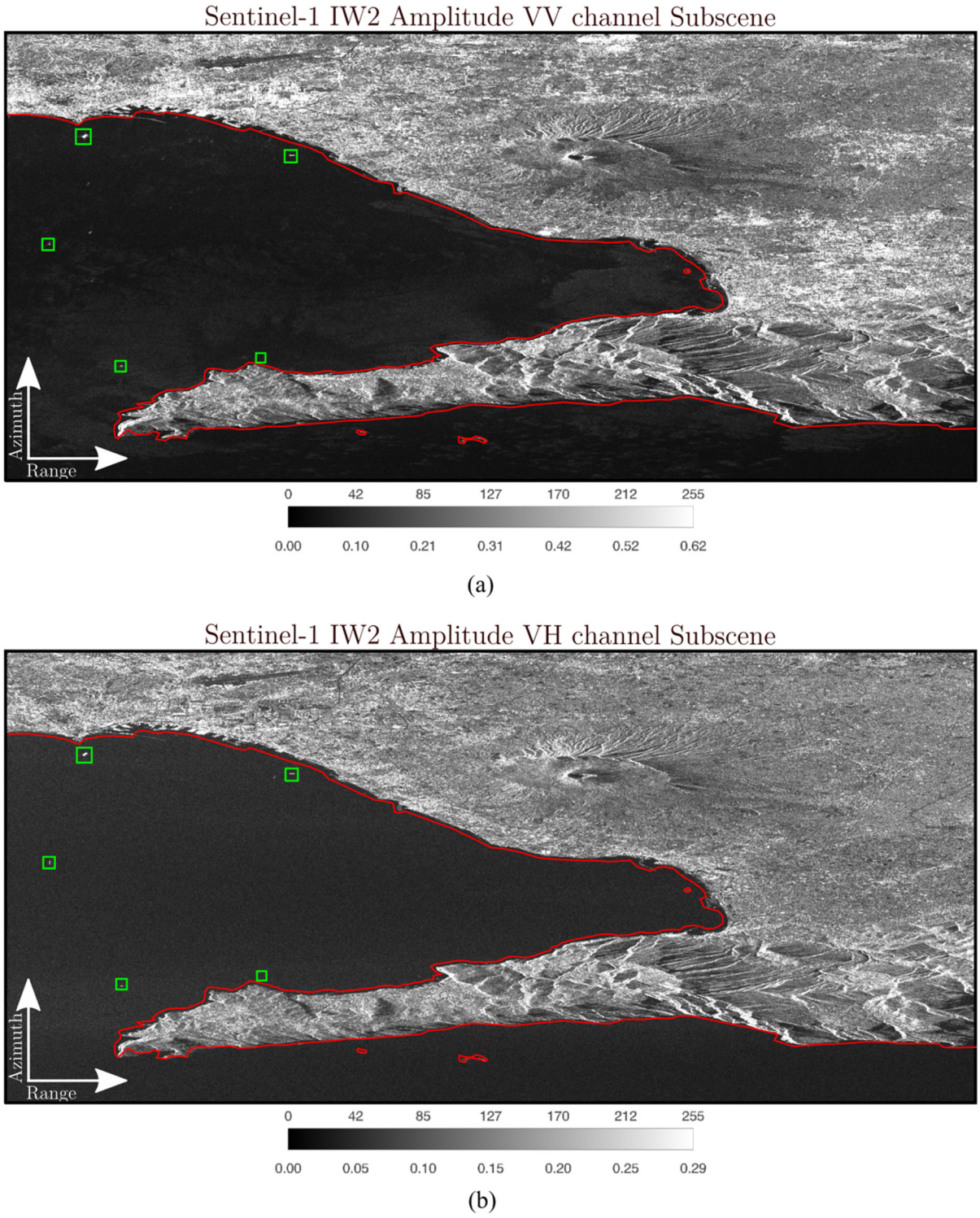

Fig. 12. Gulf of Naples. Subscene extracted from the complex IW2 subswath in range–azimuth coordinates with the coastline in red and ships identified via AIS as green squares. (a) The calibrated amplitude of the co-polarization channel. (b) The calibrated amplitude of the cross-polarization channel.

The estimation window size used to calculate (3) is 5×3 (range $\times$ azimuth) to take into account the higher resolution in range.

In Figs. 12 and 13, the symmetry parameter r image [Fig. 13(a)] is compared with the amplitude of the co-polarization and cross-polarization channel images [Fig. 12(a) and (b), respectively]. Since to retrieve r a window estimation has been used (hence the speckle is also reduced), a boxcar filter of the same size has been applied when processing individually the co-polarization and cross-polarization images.

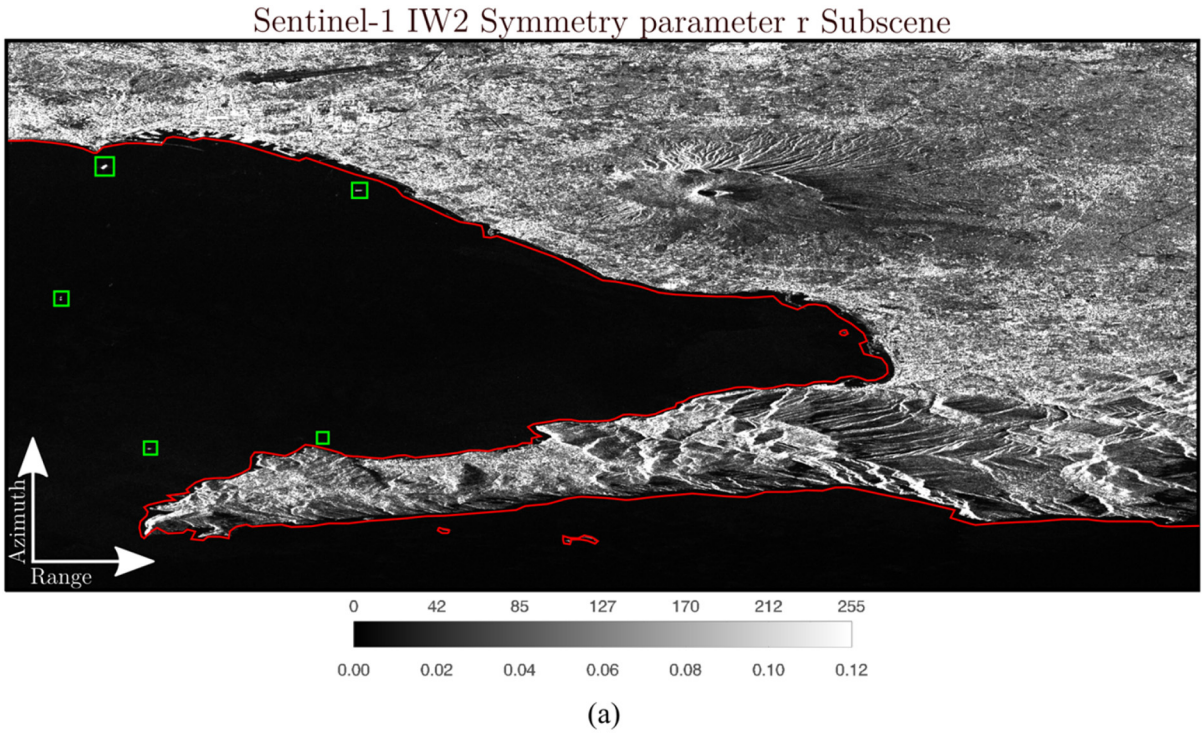

Fig. 13. Gulf of Naples. The coastline is shown in red, and ships identified via AIS are shown as green squares. (a) Estimated symmetry parameter r using 5×3 (range $\times$ azimuth) window. (b) Binary output based on the threshold th.

The binary mask in Fig. 13(b) is obtained by thresholding the r image using the following empirical relation:

$$th = mean\left(r_{\text{ocean}}\right) + 3 * stddev\left(r_{\text{ocean}}\right) \tag{4}$$

where r_{ocean} is an image layer obtained from r after masking out the land, $mean(\cdot)$ and $stddev(\cdot)$ provide the average and standard deviation value of unnormalized correlation r over the ocean, and th is the global threshold. Land masking has been performed with the help of auxiliary data provided by the SRTM water body data set. Equation (4) is reasonable since the amount of ship pixels is negligible compared to the amount of ocean pixels.

B. Entropy Approach

Because (1) is a Hermitian positive–definite matrix, the H2α dual-polarimetric eigenvalues decomposition theorem is applied to retrieve the entropy H [29]

$$H = -\sum_{I=1}^{2} P_i \log_2\left(P_i\right) \tag{5}$$

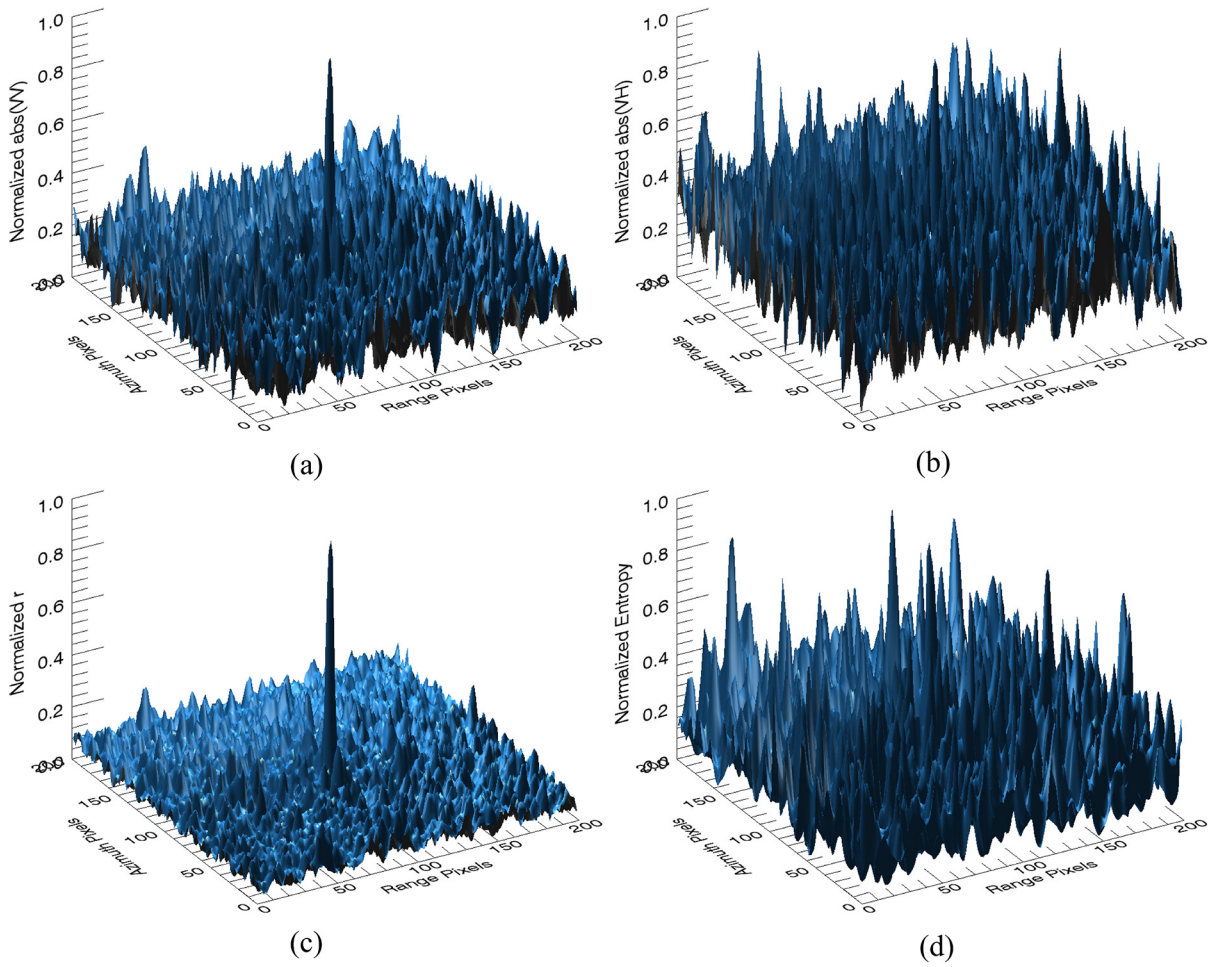

Fig. 14. Three-dimensional representation of the normalized parameters used for comparison: (a) VV polarization; (b) VH polarization; (c) r based; and H based.

where the probabilities P_i are defined as

$$P_i = \frac{\lambda_i}{(\lambda_1 + \lambda_2)}. \tag{6}$$

In (6), λ_1 and λ_2 (with $\lambda_1 > \lambda_2$) are indicating the eigenvalues of the covariance matrix defined in (1).

To show the behavior of the different parameters in case of small maritime targets, the fishing vessel in Fig. 9 is taken as an example. Although this target has been identified with a valid AIS message, the length is not reported.

In Fig. 14, a 200×200 pixels region of interest surrounding the fishing vessel in Fig. 9 is plotted as a surface curve for the normalized VV, VH, r, and H parameters. As a matter of fact, the r-based approach allows de-emphasizing the sea surface clutter while enhancing the maritime target, when compared to single-polarization channels. For the case analyzed, the cross-polarization channel VH and the polarimetric entropy H are not performing well since it is quite difficult to discern the target from the surrounding clutter.

V. Discussions and Conclusion

Synergetic use of multifrequency and multipolarization satellite SAR data in the framework of maritime target detection has been conducted. For this paper, high-resolution C-band dual-polarization VV/VH IWS mode from recently launched Sentinel-1A satellite and very-high-resolution X-band single-polarization HH StripMap mode from TerraSAR-X satellite have been used. Two regions in southern Italy have been imaged by the two satellites almost at the same time and the same orbit path, although placed in two different orbital heights. Maritime targets detected by the SAR imagery have been augmented by ground truth measurements provided by AIS messages collected in the monitored area. Satellite wind speed measurements have been used to get an indication of the met-ocean conditions and motivate some observations.

In the first part of the paper, the assessment of the operational IWS C-band Sentinel-1 with StripMap X-band TerraSAR-X data and their synergetic use were addressed. In particular, three interesting cases have been chosen because these are relevant for maritime surveillance applications: 1) monitoring of harbor area; 2) analysis of ships and ship wake signatures; and 3) surveillance of small boats without AIS. The joint use of the two satellites working at two different frequencies enables applications such as target-type discrimination, moving/nonmoving target differentiation, and moving target speed estimation. It is worth mentioning that only the comparison for the purposes of maritime target observation has been addressed here, although very interesting met-ocean signature differences are also observable between the C- and X-band data sets, e.g.,

the oceanic and atmospheric signature (Fig. 8, top-left corners) and the internal waves signature (Fig. 10, center scenes).

In the second part of the paper, multipolarization analysis of the C-band data set was carried out. Results using the reflection symmetry approach confirmed previous experiences on other C-band and X-band satellite data. From the first analysis conducted here on Sentinel-1A data, the reflection symmetry parameter performed better than single-pol features and dual-polarimetric entropy. A final validation and comparison with other polarimetric detectors is, however, to be done in future work.

ACKNOWLEDGMENT

The authors would like to thank the European Space Agency (ESA) for providing Sentinel-1A data free of charge via Scientific Data Hub (https://scihub.esa.int/). TerraSAR-X data were provided by the German Aerospace Center (DLR) via the scientific announcement of opportunity proposal OCE1045. The views, opinions, and findings contained in this paper are those of the authors and should not be construed as an official DLR's position, policy, or decision.

REFERENCES

[1] ESA Communications "Sentinel-1: ESA's Radar Observatory Mission for GMES Operational Services", 2012.
[2] E. Attema *et al.*, "Sentinel-1—The radar mission for GMES operational land and sea services," *ESA Bull.*, vol. 131, pp. 10–17, 2007.
[3] S. Lehner *et al.*, "Ship surveillance with high resolution Terrasar-X satellite in African waters," *Remote Sensing of the African Seas*, New York, NY, USA: Springer-Verlag, 2014, pp. 285–313.
[4] R. Touzi, P. W. Vachon, and J. Wolfe, "Requirement on antenna cross-polarization isolation for the operational use of C-band SAR constellations in maritime surveillance," *IEEE Geosci. Remote Sens. Lett.*, vol. 7, no. 4, pp. 861–865, Oct. 2010.
[5] F. Nunziata, M. Migliaccio, and C. E. Brown, "Reflection symmetry for polarimetric observation of man-made metallic targets at sea," *IEEE J. Ocean. Eng.*, vol. 37, no. 3, pp. 384–394, Jul. 2012.
[6] D. Velotto, F. Nunziata, M. Migliaccio, and S. Lehner, "Dual-polarimetric terrasar-x SAR data for target at sea observation," *IEEE Geosci. Remote Sens. Lett.*, vol. 10, no. 5, pp. 1114–1118, Sep. 2013.
[7] International Convention for the Safety of Life at Sea (SOLAS), Chapter V: Safety of Navigation, Annex 17 – Automatic Identification Systems (AIS), 2002 [Online]. Available: www.imo.org.
[8] Commission of the European Communities "Common position adopted by the council with a view to the adoption of a directive of the European Parliament and of the council amending directive 2002/59/EC establishing a community vessel traffic monitoring and information system", Jun. 2008.
[9] P. Brandt, A. Rubino, W. Alpers, and J. O. Backhaus, "Internal waves in the strait of messina studied by a numerical model and synthetic aperture radar images from the ERS 1/2 satellites," *J. Phys. Oceanogr.*, vol. 27, no. 5, pp. 648–663, 1997.
[10] S. Brusch *et al.*, "Ship surveillance with TerraSAR-X," *IEEE Trans. Geosci. Remote Sens.*, vol. 49, no. 3, pp. 1092–1103, Mar. 2011.
[11] A. Monti Guarnieri, "Adaptive removal of azimuth ambiguities in SAR images," *IEEE Trans. Geosci. Remote Sens.*, vol. 43, no. 3, pp. 625–633, Mar. 2005.
[12] M. Villano and G. Krieger, "Spectral-based estimation of the local azimuth ambiguity-to-signal ratio in SAR images," *IEEE Trans. Geosci. Remote Sens.*, vol. 52, no. 5, pp. 2304–2313, May 2014.
[13] G. Di Martino, A. Iodice, D. Riccio, and G. Ruello, "Filtering of azimuth ambiguity in stripmap synthetic aperture radar images," *IEEE J. Sel. Top. Appl. Earth Obs. Remote Sens.*, vol. 7, no. 9, pp. 3967–3978, Sep. 2014.
[14] C. Wang, Y. Wang, and M. Liao, "Removal of azimuth ambiguities and detection of a ship: Using polarimetric airborne C-band SAR images," *Int. J. Remote Sens.*, vol. 33, no. 10, pp. 3197–3210, May 2012.
[15] D. Velotto, M. Soccorsi, and S. Lehner, "Azimuth ambiguities removal for ship detection using full polarimetric X-band SAR data," *IEEE Trans. Geosci. Remote Sens.*, vol. 52, no. 1, pp. 76–88, Jan. 2014.
[16] D. Velotto, C. Bentes, B. Tings, and S. Lehner, "Comparison of Sentinel-1 and TerraSAR-X for ship detection," *Proc. IEEE Int. Geosci. Remote Sens. Symp.*, 2015, pp. 3282–3285.
[17] G. Saur *et al.*, "Detection and classification of man-made offshore objects in TerraSAR-X and rapideye imagery: Selected results of the demarine-DEKO project," *Proc. IEEE OCEANS Conf.*, 2011, DOI: 10.1109/Oceans-Spain.2011.6003596.
[18] A. O. Knapskog, S. Brovoll, and B. Torvik, "Characteristics of ships in harbour investigated in simultaneous images from TerraSAR-X and PicoSAR," *Proc. IEEE Radar Conf.*, 2010, pp. 422–427.
[19] G. Margarit, J. J. Mallorqui, J. Fortuny-Guasch, and C. Lopez-Martinez, "Phenomenological vessel scattering study based on simulated inverse SAR imagery," *IEEE Trans. Geosci. Remote Sens.*, vol. 47, no. 4, pp. 1212–1223, Apr. 2009.
[20] A. Soloviev, M. Gilman, K. Young, S. Brusch, and S. Lehner, "Sonar measurements in ship wakes simultaneous with TerraSAR-X overpasses," *IEEE Trans. Geosci. Remote Sens.*, vol. 48, no. 2, pp. 841–851, Feb. 2010.
[21] N. R. Stapleton, "Ship wakes in radar imagery," *Int. J. Remote Sens.*, vol. 18, no. 6, pp. 1381–1386, 1997.
[22] K. Eldhuset, "An automatic ship and ship wake detection system for spaceborne SAR images in coastal regions," *IEEE Trans. Geosci. Remote Sens.*, vol. 34, no. 4, pp. 1010–1019, Apr. 1996.
[23] J. K. Tunaley, "The estimation of ship velocity from SAR imagery," *Proc. IEEE Int. Geosci. Remote Sens. Symp.*, 2003, vol. 1, pp. 191–193.
[24] P. W. Vachon, J. W. M. Campbell, C. A. Bjerkelund, F. W. Dobson, and M. T. Rey, "Ship detection by the RADARSAT SAR: Validation of detection model predictions," *Can. J. Remote Sens.*, vol. 23, no. 1, pp. 48–59, 1997.
[25] C. Bentes, D. Velotto, and S. Lehner, "Analysis of ship size detectability over different TerraSAR-X modes," *Proc. IEEE Int. Geosci. Remote Sens. Symp.*, 2014, pp. 5137–5140.
[26] B. Tings, C. A. B. da Silva, and S. Lehner, "Dynamically adapted ship parameter estimation using TerraSAR-X images," *Int. J. Remote Sens.*, Aug. 2015, DOI:10.1080/01431161.2015.1071898.
[27] P. W. Vachon, J. Wolfe, and H. Greidanus, "Analysis of Sentinel-1 marine applications potential," *Proc. IEEE Int. Geosci. Remote Sens. Symp.*, 2012, pp. 1734–1737.
[28] R. Touzi, "On the use of polarimetric SAR data for ship detection," *Proc. IEEE Int. Geosci. Remote Sens. Symp.*, 1999, vol. 2, pp. 812–814.
[29] S. Cloude, "The dual polarization entropy/alpha decomposition: A PALSAR case study," *ESA Special Publ.*, vol. 644, p. 2, 2007.

Domenico Velotto (M'15) was born in Italy, on April 30, 1981. He received the M.Sc. degree (five-year legal course of study) in nautical science (curriculum electronic radio-navigation and Earth observation systems) from the Università degli Studi di Napoli "Parthenope," Napoli, Italy, in 2008.

In 2009, he joined the Synthetic Aperture Radar (SAR) Oceanography Group, Remote Sensing Technology Institute (MF), German Aerospace Center (DLR), Weßling, Germany, as a Ph.D. student. Since 2013, he has been a Research Assistant at the Maritime Security Lab, DLR, Bremen, Germany. His main research interests deal with electromagnetic models, image processing, and Earth observation with SAR polarimetry with emphasis on oil spill and maritime targets detection and classification.

Carlos Bentes was born in Volta Redonda, Brazil, in 1983. He received the B.S.E.E. and M.S.E.E. degrees from the Instituto Tecnológico de Aeronáutica (ITA), São José dos Campos, Brazil, in 2007 and 2012, respectively.

Since 2013, he has been a Research Assistant at the German Aerospace Center (DLR), Bremen, Germany, in the field of remote sensing. His professional interests and research areas encompass information mining, machine learning, signal processing, and remote sensing applications.

Björn Tings received the B.S. degree in scientific programming and his simultaneous qualification in mathematical-technical software development in 2010 and the M.Sc. degree in artificial intelligence in 2013, both from Aachen University, Aachen, Germany.

During his B.S. studies and during the first year of his M.S. studies he gained practical experience working for the Laboratory for Machine Tools and Production Engineering (WZL), RWTH Aachen University, Aachen, Germany. For his M.S. thesis, he specialized on image processing and pattern recognition in the fields of avionic and defense. Since 2013, he has been a Research Assistant at the Institute for Remote Sensing Technology (IMF), German Aerospace Center (DLR), Bremen, Germany. In IMF's Maritime Safety and Security Lab (FMS) in Bremen, Germany, his research is focused on developing algorithms for detection and classification of ships on synthetic aperture radar (SAR) satellite images. As an interface between the FMS and the satellite data receiving ground station in Neustrelitz, Germany, he is also responsible for the operationalization of research results into NRT-capable SAR data processors.

Susanne Lehner studied mathematics and physics at the University of Hamburg, Hamburg, Germany. She received the M.Sc. in applied mathematics from Brunel University, Uxbridge, U.K., in 1979 and the Ph.D. degree in geophysics from the University of Hamburg, Hamburg, Germany, in 1984.

During the Ph.D., she worked as a Research Scientist at the Max-Planck Institute for Meteorology, Hamburg, Germany. She joined the German Aerospace Center DLR/DFD in 1996. Since 1999, she has been head of the team Radar Oceanography at the Institute for Remote Sensing Technology (IMF), DLR, Oberpfaffenhofen, Germany. In SAR oceanography, her research focused on developing algorithms to extract information on wind fields, sea state, currents, and underwater topography from SAR images. Her recent interest, in addition to global sea state measurements, is in high-resolution coastal SAR oceanography, especially TerraSAR-X oceanography and meteo-marine observations, and maritime traffic surveillance in near real time. She holds a faculty position at the Nova Southeastern University, Port Everglades, FL, USA. She was appointed as Affiliated Faculty Member in 2013. Currently she is head of the Maritime Security Lab, Bremen, Germany, established in July 2013.